Imaging in the presence of grain noise using the decomposition of the time reversal operator

E. Kerbrat, C. Prada, D. Cassereau, and M. Fink
Laboratoire Ondes et Acoustique, ESPCI, Université Paris VII, UMR CNRS 7587, 10 rue Vauquelin, 75005 Paris, France

(Received 15 April 2002; revised 25 November 2002; accepted 17 December 2002)

In this paper, we are interested in detecting and imaging defects in samples of cylindrical geometry with large speckle noise due to the microstructure. The time reversal process is an appropriate technique for detecting flaws in such heterogeneous media as titanium billets. Furthermore, time reversal can be iterated to select the defect with the strongest reflectivity and to reduce the contribution of speckle noise. The DORT (the French acronym for Decomposition of the Time Reversal Operator) method derives from the mathematical analysis of the time reversal process. This detection technique allows the determination of a set of signals to be applied to the transducers in order to focus on each defect separately. In this paper, we compare three immersion techniques on a titanium sample, standard transmit/receive focusing, the time reversal mirror (TRM), and the DORT method. We compare the sensitivity of these three techniques, especially the sensitivity to a poor alignment of the array with the front face of the sample. Then we show how images of the sample can be obtained with the TRM and the DORT method using backpropagation algorithm. [DOI: 10.1121/1.1548156]

PACS numbers: 43.20.Gp, 43.20.Bi [DEC]

I. INTRODUCTION

Most applications in nondestructive testing require the focusing of ultrasonic waves inside the investigated medium in order to detect minor defects. The detection of weak flaws is especially difficult when the inspected object is heterogeneous[1] and has complex geometry.[2] The weak echo from the defect can be masked by the speckle due to the microstructure and the complex geometry significantly degrades the propagation of ultrasound in the area of interest. In many applications, the solid sample is immersed in water and one or several transducers are moved to scan the area of interest. Different approaches have been extensively studied in order to produce an ultrasonic focused beam through complex liquid–solid interfaces. In the simplest approach, the beam focusing is achieved with one transducer whose geometry is matched to the liquid–solid interface and the desired focal point.[3] Thus, the focusing process is improved allowing a better signal-to-noise ratio and also a greater resolution assisting the separation of close defects and flaw sizing. However, the inspection of thick samples requires the use of several transducers of different geometries in order to scan through the whole sample. This step-by-step scanning is also extremely time consuming. Last but not least, a misadjustment of the focused transducer significantly degrades the detection quality. This bad positioning is frequently observed, especially for large samples when the focused transducer is translated over a long distance.

A second technique based on the use of multielement transducer arrays gives a greater flexibility.[4] Transducer arrays are connected to a set of electronic time delays whose values are adapted to focus in both the transmit and receive modes. The combination of transmit and receive focusing allows the achievement of high resolution.

Another technique, called SAFT[5,6] (Synthetic Aperture and Focusing Technique) is based on the coherent summation of multiple data obtained from the sample, from a large number of transducers positions.

However, all these techniques require some prior knowledge of the geometry and of the acoustics properties of the solid sample.

Here, we are interested in detecting and imaging the defect in titanium billets used in the aerospace industry. Such samples are heterogeneous media and the polycrystalline microstructure yields a strong scattering noise,[7] which can hide the echo from a defect.

To solve the detection problems due to the heterogeneous structure and the geometry of the sample, another technique has been developed in our laboratory. Relying on the time reversal invariance of the acoustic propagation, this technique uses a time reversal mirror[8,9] (TRM). Such a TRM can convert a divergent wave, scattered by a defect, into a convergent wave focused on the defect, by emitting a time reversed version of the received wave field. It is a self-focusing technique[10] that compensates for distortions of the ultrasonic wave due to the geometry of the liquid–solid interface and to the microstructure of the sample.[11]

When the sample contains only one defect, after a time reversal (TR) process, an optimal focusing is obtained on the flaw, without the need for any assumptions concerning the geometry of the sample and the ultrasonic celerity. In the presence of speckle noise, the iteration of the TR operation allows the separation of the echo of a weak, deep defect from the speckle noise.[12] If the sample contains several defects, several iterations of the TR process leads to focusing on the strongest flaw.[12,13]

Parallel to the implementation of a detection procedure using time reversal mirrors, we have developed another detection technique called the DORT (the French acronym for

Decomposition of the Time Reversal Operator) method. This method is based on the decomposition of the time reversal operator that was introduced to describe the iterative time reversal process.[13] Similar to the time reversal process only rough assumptions need to be made on the ultrasound velocity and the geometry of the medium.

The DORT method has been used to separate the responses from different scatterers in a wave guide,[14] through inhomogeneous media,[15] and also in thin plates using Lamb waves.[16] It has also been applied to the separation and characterization of Lamb waves circumnavigating a shell.[17]

The goal of this paper is to show that the DORT method can be efficiently applied in nondestructive testing. In particular, we show that the DORT method can be used to enhance and separate the echo of a weak scatterer from speckle noise. In order to evaluate the potentials of this technique, we compare it to classical focusing and to the time reversal process.

The DORT method and the time reversal process are then combined with numerical backpropagation of the data in order to reconstruct an image of the medium. This backpropagation is calculated using the simulation code PASS that takes into account the geometry of the transducers as well as the solid–liquid interface.[18] Thus, it requires some prior knowledge of the sample.

II. EXPERIMENTAL SETUP

The three detection techniques have been compared using the same setup: a cylindrical titanium sample with defects, and a transducer array connected to a multichannel electronic system including programmable transmitters.

A. The transducer array and the electronic prototype

Experiments are realized with a ''Fermat surface'' transducer array whose geometry is adapted to make all the propagation times equal from the transducer surface to a point at 140 mm depth in the inspected sample, thus providing optimum focusing at this point. The array of transducers is prefocused at 140 mm in the titanium billet of 250 mm diameter with a 55 mm deep water column. This array is made of 121 transducers working at 5 MHz, with a bandwidth equal to 70%. The transducer elements, having the same area, are distributed according to a six annuli structure of, respectively, 1, 8, 16, 24, 32, and 40 elements (Fig. 1).

The 121 elements are connected to an electronic system allowing transmission and acquisition of the experimental data for the three detection tests at a sampling rate of 40 MHz. The transmission module is made of 121 programmable transmitters. This enables us to emit and to record any kind of temporal signal on each transducer of the array.

B. The inspected solid sample

The inspected medium is a Ti6-4 titanium alloy cylindrical sample (Fig. 2), immersed in water, that contains three flat bottom holes (FBH). These defects of diameters 0.8, 0.4, and 0.5 mm are located at a depth of 140 mm and spaced 15 mm apart. The longitudinal wavelength in the titanium sample is 1.2 mm at 5 MHz and the transverse resolution at 140 mm inside the material is 3.3 mm at -6 dB. Thus, the defects are well resolved and can be considered as points.

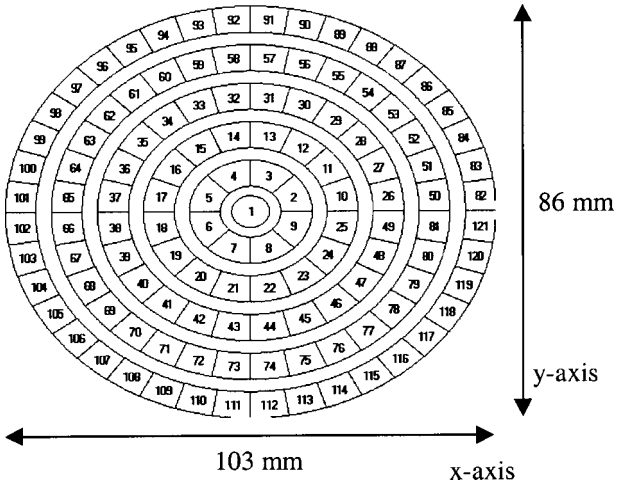

FIG. 1. Geometry of the transducer array.

III. THE TIME REVERSAL MIRROR AND THE DORT METHOD PRINCIPLE

The time reversal process and the DORT method which have been presented in several papers[8–18] are briefly reviewed in this section.

A. "Conventional" time reversal

A time reversal process allows the conversion of a divergent wave emerging from a source into a wave focusing on the source. In our case, the source is a flat bottom hole whose position is unknown. The time reversal process is an adaptive focusing technique that requires the following three steps:

(1) Transmission of a short widely divergent wave by several elements of the array; for this particular application, it was established that 25 central transducers was a good compromise.

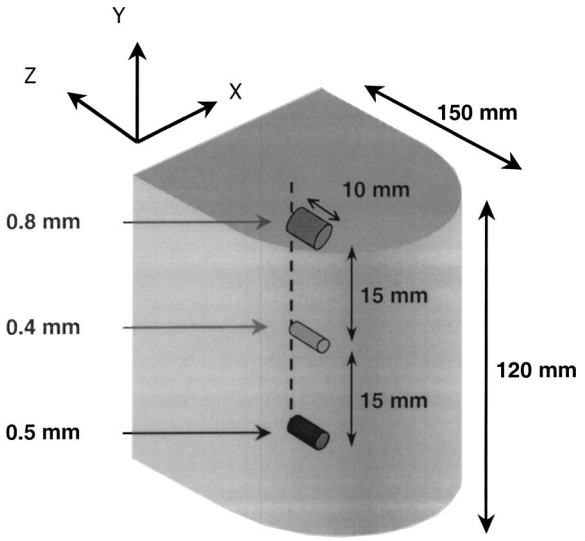

FIG. 2. The titanium sample.

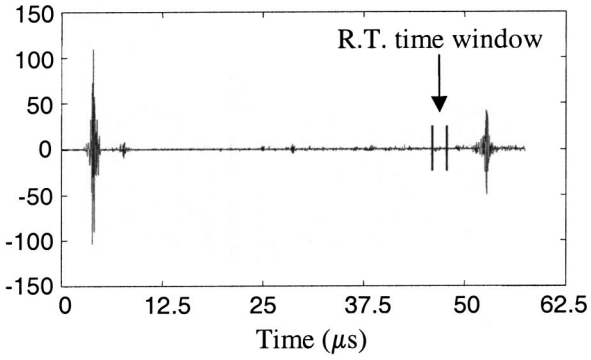

FIG. 3. Time reversal and DORT window.

(2) The wave reflected by the defect is detected by the array and the echographic signals are recorded in the memories of the electronic system.
(3) These signals are then time reversed and used to transmit a wave focusing on the flaw. The time reversal process is performed on a 0.8 μs time window corresponding to the depth of the defect (Fig. 3).

In this paper, we study the temporal signals recorded by the TRM after two iterations. Let us describe two treatments applied to these signals. Because of 16 defective channels on the electronic system, only 105 signals are exploited. First, we present the incoherent summation $\mathrm{Inc}(t)$[11,12] of the 105 linear signals $[f_k(t)]_{1\leqslant k\leqslant 105}$, determined according to the summation

$$\mathrm{Inc}(t)=\sum_{k=1}^{105} f_k(t), \tag{1}$$

where $f_k(t)=R_{2,k}(t)$ is the ultrasonic signal recorded on the transducer k at the second iteration. This process is called ''incoherent summation'' [Eq. (1)] because the individual data are not in phase.

Another compact presentation of the time reversal process is the ''iterative coherent summation'' $\mathrm{Coh}(t)$ [Eq. (2)] of the linear signals $[f_k(t)]_{1\leqslant k\leqslant 105}$, determined according to the summation

$$\mathrm{Coh}(t)=\sum_{k=1}^{105} f_k(t-\tau_k), \tag{2}$$

where the delay τ_k is the time when the signal $R_{1,k}(t)$ recorded at the first iteration is the maximum. For a zone containing a defect, this process will greatly enhance the signal from the defect, even if it is not at the array focus. Examples of these two representations will be given in Sec. IV B.

B. The DORT method

The DORT method has been described in several papers.[13–15,17,18] This method is derived from the theoretical analysis of time reversal mirrors. It is based on a matrix formalism that describes a transmit–receive process performed with an array of L transducers. Such an array insonifying a given medium is a linear and time invariant input–output system characterized by $L\times L$ interelement impulse responses $k_{lm}(t)$ defined as the output of the element number l when the input of the element number m is a delta impulse. At a given frequency, the $L\times L$ transfer matrix $K(\omega)=[K_{lm}(\omega)]_{1<l,m<L}$ can be calculated by the Fourier transform of the responses $k_{lm}(t)$.

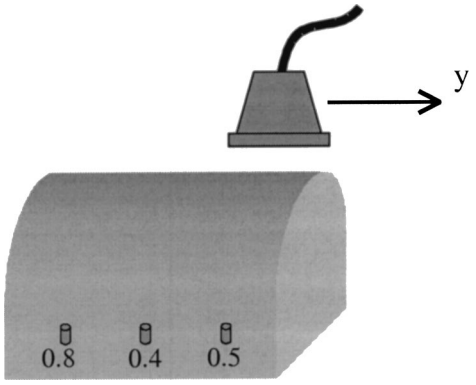

FIG. 4. Translation of the array along the y axis.

The time reversal operator, defined as $K^*(\omega)K(\omega)$, can be diagonalized. In general, the number of significant eigenvalues is equal to the number of well-resolved pointlike defects in the medium and each significant eigenvector of the time reversal operator is associated with one of the defects. The associated eigenvalue depends on the reflectivity of the defect and also on its position relative to the array. The first eigenvector generally corresponds to the strongest reflector and contains the signals that would be obtained after a large number of time reversal iterations.

In practice, the diagonalization of $K^*(\omega)K(\omega)$ is obtained from the calculation of the singular value decomposition (SVD) of the transfer matrix $K(\omega)$ [Eq. (3)],

$$K(\omega)=U(\omega)S(\omega)^tV^*(\omega), \tag{3}$$

where $S(\omega)$ is a real diagonal matrix of singular values. $U(\omega)$ and $V(\omega)$ are unitary matrices. The eigenvalues of $K^*(\omega)K(\omega)$ are the squares of the singular values of $K(\omega)$ and its eigenvectors are the columns of $V(\omega)$.

In summary, the DORT method consists of the measurement of the interelement impulse response functions $k_{lm}(t)$, the analysis of the singular values of the transfer matrix $K(\omega)$ and possibly the backpropagation of the eigenvectors associated with the most significant singular values.

IV. DETECTION IN A TITANIUM ALLOY SAMPLE

This part concerns the detection of the flat bottom holes in the titanium sample described above and illustrates the sensitivity of each technique to a bad positioning of the array.

For each technique, the input signal is a sine wave at 5 MHz modulated by a 1 μs Gaussian function. This signal is applied to one or several transducer(s) depending on the technique.

A first set of measurements is made to detect the three flaws. To this end, the array which is prefocused at the depth of the defects (Fig. 4), is translated parallel to the y axis in 1 mm steps.

A second set of measurements is made to test the robustness of each technique to a misalignment of the probe, that is

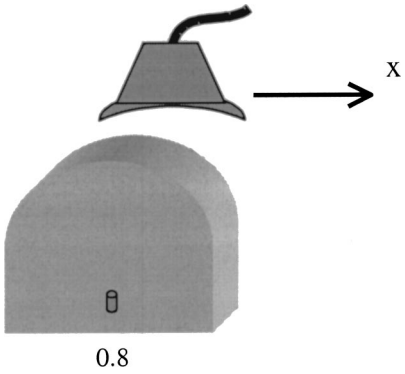

FIG. 5. Translation of the array along the x axis.

to say when the probe is no longer aligned with the liquid–solid interface. This is done for the 0.8 mm flaw by displacement of the array along the x axis (Fig. 5). The defect is initially at the array focus corresponding to $x=0$ mm. The data are acquired after translating the array along the x axis, by 0.1 mm steps and for $-3\ \text{mm} \leqslant x \leqslant 3\ \text{mm}$.

We first present the performance of the focusing technique in transmit–receive mode as if using a single large focused transducer.

A. Focusing in transmit–receive mode

The measurements are realized with the transducer array described in Sec. II but in order to simulate a single large focused transducer, the elements are fired simultaneously by the same input signal (focusing in transmit mode).

1. Detection of the three defects with the geometrical focusing (translation ∥ y)

For a given position of the array along the y axis, the received signals $[S_k(y,t)]_{1\leqslant k\leqslant 105}$ are stored on each channel during 4 μs and summed to simulate a unique large transducer

$$A(y,t)=\sum_{k=1}^{105} S_k(y,t). \tag{4}$$

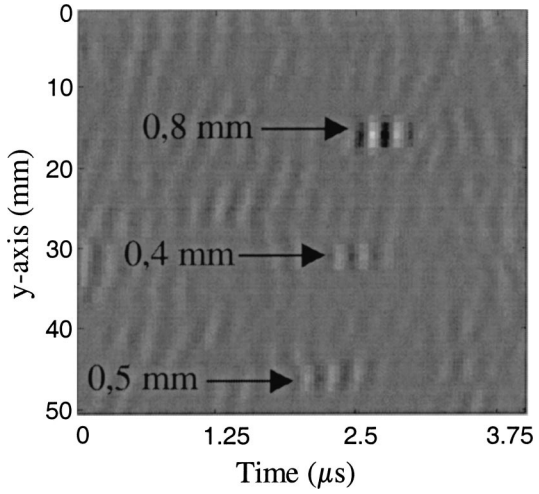

FIG. 6. Detection of the three defects with the focusing in transmit–receive mode.

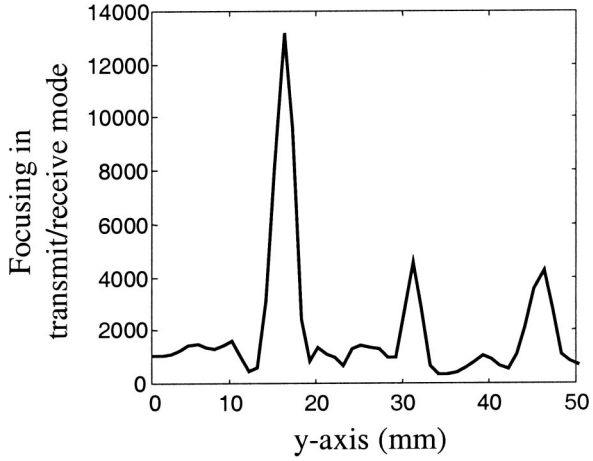

FIG. 7. Detection of the three defects with the focusing in transmit–receive mode at the depth of the defects on an 800 ns time window.

The function $A(y,t)$ is displayed in Fig. 6. The echoes from the 0.8 mm, 0.4 mm, and 0.5 mm defects are visible between 2 and 3 μs for the positions $y=16$, 31, and 46 mm, respectively. As can be seen on the figure, the array displacement is not perfectly parallel to the billet axis.

We then calculate the maximum of $A(y,t)$, defined as $M(y)$, for an 800 ns time window corresponding to the depth of the flaws and written as follows [Eq. (5)]:

$$M(y)=\max[A(y,t)]. \tag{5}$$

The function $M(y)$ is displayed at Fig. 7. The defects are well detected with a signal-to-noise ratio equal to 19, 10, and 9.5 dB for the 0.8, 0.5, and 0.4 mm flat bottom holes, respectively. The drawback of this focusing technique is that, due to the focused transmitted signal, a defect is detected by the transducer only when it is close to the focal point. Furthermore, as shown in the next paragraph, a misalignment of the transducer relative to the liquid–solid interface strongly degrades the focusing process.

2. Robustness of the geometrical focusing (translation ∥ x)

In this paragraph, we evaluate the detection quality of the 0.8 mm flaw with focusing in transmit–receive mode, after displacement of the array along the x axis (Fig. 5). The elements are simultaneously fired by the same input signal as before. The 105 signals are then acquired on an 800 ns time window corresponding to the defect position. This measurement is repeated after translating the array along the x axis. The association of a time window to a particular depth is possible because the array is prefocussed in the inspected area, which of course requires some knowledge on the sample's average acoustic properties.

We then calculate the $M(x)$ term [Eq. (5)], on an 800 ns time window corresponding to the depth of the flaw, for the 61 positions of the transducer (Fig. 8). The decrease of the detection level is equal to 11 dB after translating the array for a 0.5 mm distance. Note that the degradation observed in Fig. 8 is not perfectly symmetrical relative to the position $x=0$ mm, probably meaning a little asymmetry of the geometry.

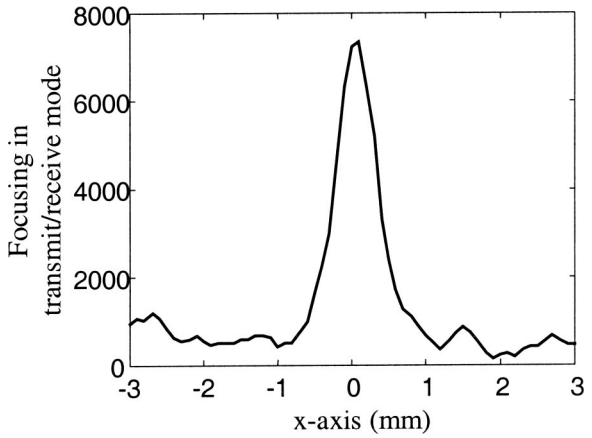

FIG. 8. Detection of the 0.8 mm defect with the focusing in transmit–receive mode along the *x* axis.

B. The conventional time reversal process

The time reversal mirror has been described in the Sec. III A. For the first transmission, the 25 central transducers are simultaneously fired by a short pulse. The time reversal process is performed on an 800 ns time window corresponding to the depth of the defects and the ultrasonic signals (B-Scan) are taken from the second iteration.

1. Detection of the three defects with the TRM (translation ∥ y)

Figure 9 displays the B-Scan measured at the second iteration when the 0.8 mm FBH is located 4 mm out of the array focus. The undulation of the wavefront reveals the out of focus position of the defect. The measurement of the B-Scan is done by translating the array along the *y* axis by 1 mm step (Fig. 4).

The Inc(y,t) and Coh(y,t) terms [Eqs. (1) and (2)] are calculated and we represent (Fig. 10) the peak of each summation for an 800 ns time window adapted to the depth of the defects. Three maxima are observed for $y=16$, 31, and 46 mm, associated with the flaws of 0.8, 0.4, and 0.5 mm diameter, respectively. The amplitude of each maximum is related to the size of the corresponding defect. The coherent summation generates three maxima wider and higher than these obtained with the incoherent summation. For example, by applying the coherent summation, the 0.8 mm FBH is detected at 15 mm distance from the focus. This is a great advantage of the self-adaptative property of the TRM process.

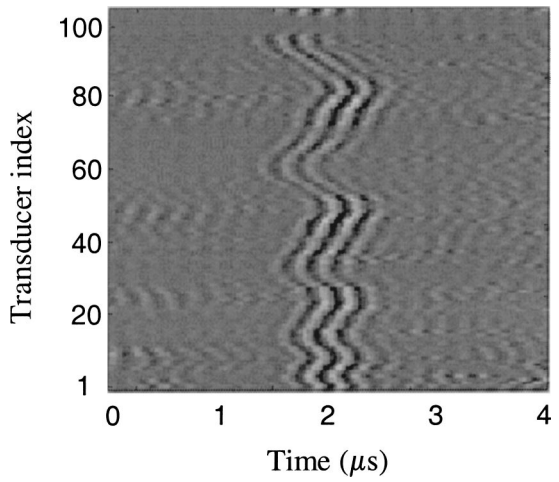

FIG. 9. Detection of the 0.8 mm defect located 4 mm from the array focus with the TRM.

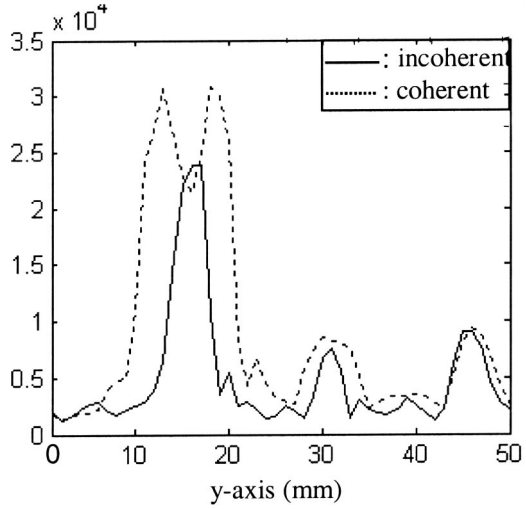

FIG. 10. Detection of the three defects with the incoherent and the coherent linear summations of the B-Scan measured with the TRM at the second iteration along the *y* axis.

2. Robustness of the TRM (translation ∥ x)

As for classical focusing, we evaluate the sensitivity of the time reversal process to a poor positioning of the transducer array relative to the titanium sample (Fig. 5). The peak in time of the Inc(x,t) and Coh(x,t) terms [Eqs. (1) and (2)] are calculated along the *x* axis (Fig. 11). They reach the maximum for $x=0$ mm, when the 0.8 mm FBH is at the focal point. Furthermore, the decrease of these incoherent and coherent summations is equal to 15 and 10 dB, respectively, after a displacement of the array for a 0.5 mm dis-

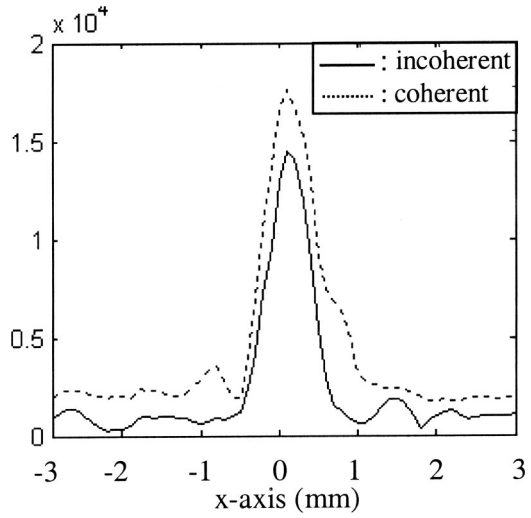

FIG. 11. Detection of the 0.8 mm defect with the incoherent and the coherent linear summations of the B-Scan measured with the TRM at the second iteration along the *x* axis.

tance. These compact representations emphasize the great advantage of the coherent summation for flaw detection out of the array focus.

These measurements were also made with nine transducers (the central transducer and the first crown) and one transducer (the central transducer) for the first transmission. We wondered whether the sensitivity of the time reversal process would be higher when the first transmission was less focused. In fact, for nine transducers, the results are similar to those obtained with 25 transducers whereas for one single transducer the energy transmitted is too weak and the defect never detected.

C. The DORT method

In order to evaluate the potentialities of the DORT method for flaw detection, it is applied to the titanium alloy sample in the same configuration as before (Figs. 1 and 2). The first step of the technique is the measurement of the interelement impulse responses $k_{lm}(t)$.

1. Detection of the three defects with DORT (translation ∥ y)

Figure 3 illustrates the interelement impulse response from element 10 to element 40 when the array is located in front of the 0.4 mm diameter FBH. The strong echoes coming from the front and the back faces of the titanium sample are easily visible. The transducer array is translated along the y axis by 1 mm steps (Fig. 4) and the interelement impulse responses $k_{lm}(t)$ are acquired on a wide temporal window. As the array is prefocused at 140 mm in the titanium sample, the choice of the temporal window corresponds to a slab at the same depth for each transducer.

2. Singular values at 5 MHz

The information corresponding to 140 mm depth inside the medium is selected and the transfer matrix $K(\omega)$ is calculated on an 800 ns time window. Working on such short signals is necessary to get a reasonable signal-to-noise ratio, otherwise the weak echo from the defect is drowned under the accumulation of the signal reflected by the grain structure.

The singular values are calculated at 5 MHz for each position of the array along the y axis (Fig. 12). The first singular value varies with the position of the flaws relative to the array focus. For example, the first singular value is associated with the FBH of diameter 0.8 mm, 0.4 mm, and 0.5 mm for the positions of the following array: $1\,\text{mm} \leqslant y \leqslant 25\,\text{mm}$, $26\,\text{mm} \leqslant y \leqslant 36\,\text{mm}$, $37\,\text{mm} \leqslant y \leqslant 49\,\text{mm}$, respectively. Furthermore, the differences between the three maxima reveal the different effective reflectivities of the flaws.

In particular, we can observe that the maximum associated with the 0.5 mm defect is smaller than the maximum associated with the 0.4 mm defect. This probably results from the fact that the 0.5 mm defect is not perfectly flat bottomed.

Near $y = 28\,\text{mm}$, two defects are simultaneously detected and a crossing can be observed on the two main singular values. For $y < 28\,\text{mm}$, the first and the second singular values are, respectively, associated with the 0.8 mm and the 0.4 mm defects while it is the contrary for $y \geqslant 28\,\text{mm}$.

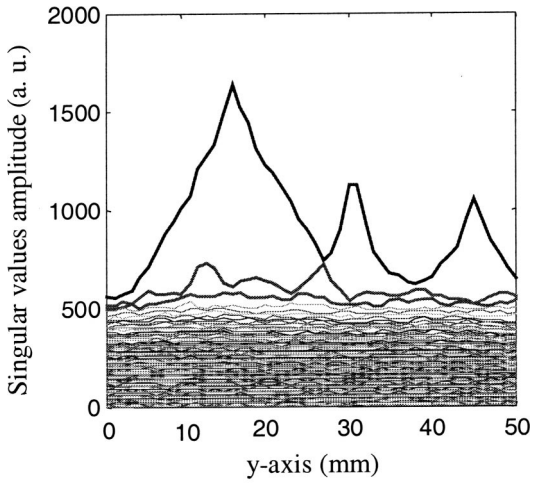

FIG. 12. Detection of the three defects with the singular values amplitude calculated at 5 MHz along the y axis.

The other singular values, called ''noise'' singular values, mostly result from the grain structure of titanium and electronic noise. Note that these ''noise'' singular values have no significant fluctuation along the y axis.

3. Frequency analysis

Until now, the study of the singular values was made at the central frequency of the transducers. However, the singular value decomposition may be done at any chosen frequency in the bandwidth of the transducer. Thus, it is interesting to observe the frequency dependence of the singular values. In our case, the SVD of the transfer matrix is calculated for the frequencies between 3.1 and 6.3 MHz at 0.16 MHz intervals.

For example, the singular values are represented when the 0.4 mm FBH is at the array focus and 5 mm out of focus, respectively (Figs. 13 and 14). For the first position, the first singular value is well separated from the others for frequencies above 4 MHz. The maximum is obtained at 5 MHz

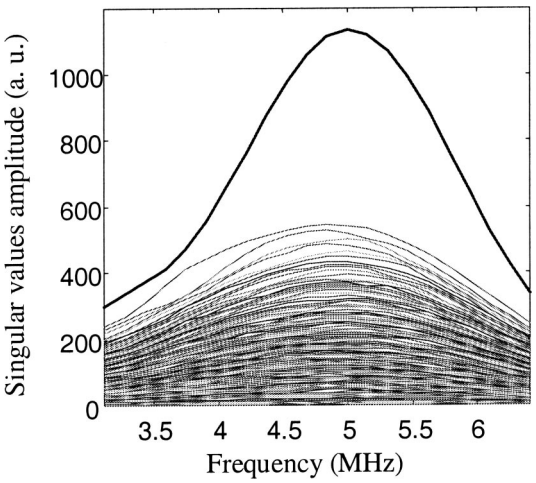

FIG. 13. Singular values amplitude when the 0.4 mm flaw is located at the array focus.

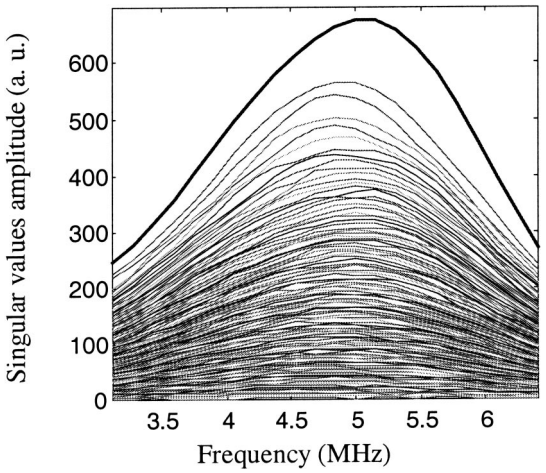

FIG. 14. Singular values amplitude when the 0.4 mm flaw is located 5 mm out of the array focus.

which is the central frequency of the transducers. When the defect is 5 mm out of focus, the first singular value associated with the defect, is closer to the other singular values.

For the second position of the defect, the first eigenvector $V_1(\omega)$ is calculated from 3.1 to 6.3 MHz with a frequency spacing equal to 0.16 MHz. Thus, the first ''temporal eigenvector'' $v_1(t)$ (Fig. 15) is obtained by inverse Fourier transform of $V_1(\omega)$. This ''temporal eigenvector'' represents the response from the defect to the array which is by reciprocity the set of signals that should be applied on each transducer in order to focus on the corresponding flaw. Although the 0.4 mm FBH is 5 mm away from the focal point, the temporal reconstruction of the first ''temporal eigenvector'' $v_1(t)$ remains associated with this defect. Indeed, the wavefront of this eigenvector shows undulating behavior which is explained by the out of focus position of the flaw.

4. Linear incoherent and coherent summations of the first temporal eigenvector $v_1(t)$

We have shown in Sec. III A a compact presentation of the time reversal process: the incoherent and coherent summations of the B-Scan acquired at the second iteration. The

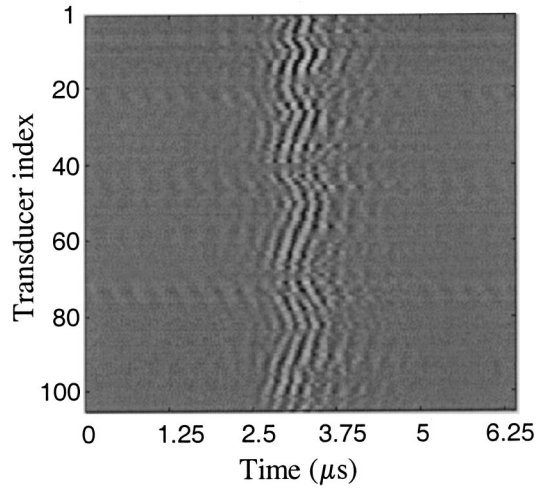

FIG. 15. First ''temporal eigenvector'' $v_1(t)$ when the 0.4 mm flaw is located 5 mm out of the array focus.

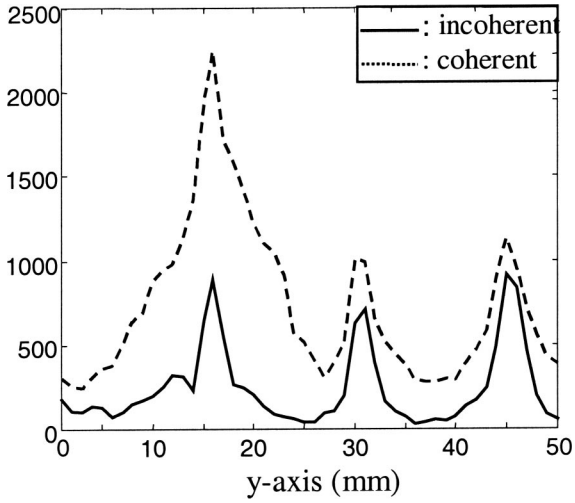

FIG. 16. Detection of the three defects with the incoherent and coherent summations of the first ''temporal eigenvector'' $v_1(t)$ calculated along the y axis.

same process is also valid for the DORT method. Indeed, it consists of calculating the linear incoherent $\mathrm{Inc}(y,t)$ and coherent $\mathrm{Coh}(y,t)$ summations of the first ''temporal eigenvector'' $v_1(t)$ obtained for each position y of the array, according to Eqs. (1) and (2). In this case, $f_k(t)=a_{1,k}(y,t)$, where $a_{1,k}(y,t)$ is the temporal signal (A-Scan) extracted from $v_1(t)$ on the transducer k. The delay τ_k introduced in Eq. (2), corresponds to the time when the signal $a_{1,k}(y,t)$ is at the maximum.

We give an example of this process in Fig. 16 which presents the peak of the $\mathrm{Inc}(y,t)$ and $\mathrm{Coh}(y,t)$ terms, calculated for each position of the array along the y axis, by 1 mm spacing. We observe on each curve, as for the first singular value (Fig. 12), three maxima for the positions $y=16$, 31, and 45 mm associated with the 0.8, 0.4, and 0.5 mm flaws, respectively. As for time reversal, the incoherent summation produces three narrow peaks whereas the effect of the coherent summation is to widen the three lobes.

5. Robustness of the DORT method (translation ∥ x)

The performances of the focusing technique in transmit–receive mode and of the TRM have been investigated in Secs. IV A and IV B when the array, initially in front of the 0.8 mm flaw ($x=0$ mm) is translated along the x axis (Fig. 5). The DORT method is now applied to the same experimental procedure.

The interelement impulse responses $k_{lm}(t)$ are measured for the 61 positions of the transducer and stored for an 800 ns time window corresponding to the depth of the defect. The transfer matrix $K(\omega)$ is then calculated and decomposed in singular values for frequencies between 3.1 and 6.3 MHz with a frequency spacing equal to 0.16 MHz.

The singular values distribution is presented at 5 MHz in Fig. 17. The maximum of the first singular value associated with the defect is obtained for $x=0$ mm, and is still significantly higher than the noise level when the defect is far from the array focus. For example, the first singular value decreases by 5 dB for a displacement of the array equal to 1.5

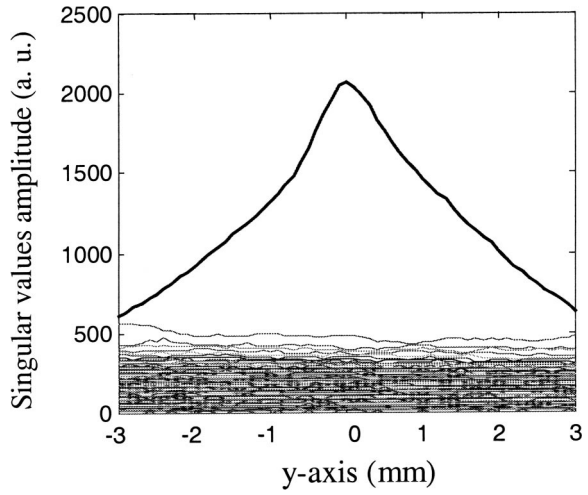

FIG. 17. Detection of the 0.8 mm flaw with the singular values amplitude at 5 MHz calculated along the x axis.

mm. Thus we see that the DORT method allows us to detect the flaw even if the transducer array is no longer adapted to the geometry of the sample.

The functions $\mathrm{Max}_t(\mathrm{Inc}(x,t))$ and $\mathrm{Max}_t(\mathrm{Coh}(x,t))$ present a maximum for $x=0.1$ and 0.2 mm, respectively (Fig. 18). Furthermore, these two terms lose 8 and 2.5 dB, respectively, for a displacement of the array equal to 0.5 mm. The coherent summation of $v_1(t)$ is a good way to break away from the loss of information when the array is no longer adapted to the geometry of the sample. Thus, it will be more interesting to analyze the coherent summation of $v_1(t)$ for a defect located out of the array axis.

This robustness is explained by the fact that for the DORT method, each transducer is fired separately, whereas the time reversal process simultaneously uses the 25 or 9 central transducers for the first transmission. Consequently, the transmission is less focused with the DORT method than with the time reversal process. Furthermore, the DORT technique takes advantage of a large angular diversity of incident

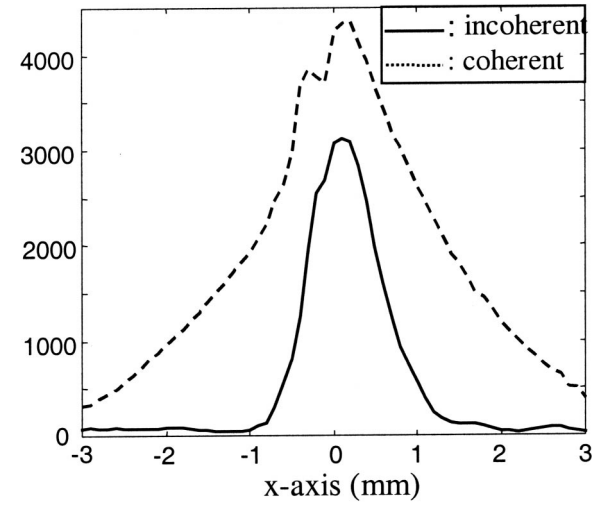

FIG. 18. Detection of the 0.8 mm flaw with the incoherent and coherent summations of the first "temporal eigenvector" $v_1(t)$ calculated along the x axis.

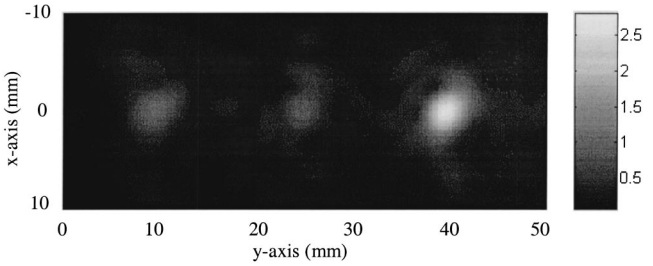

FIG. 19. Synthetic image of the sample at 140 mm depth with the time reversal mirror.

waves in the titanium sample, allowing a better detection than time reversal when the array is not perfectly aligned with the sample.

V. IMAGING IN THE TITANIUM SAMPLE

The procedures described in Sec. IV were only aimed at detecting the defects. Here, we want to make an image of the sample. To this end, we have to introduce some prior knowledge of the sample shape and we use a numerical backpropagation algorithms to reconstruct the sources of the echoes.

We propose to achieve defect localization using the simulation code PASS[18] (Phased Array Simulation Software) developed in our laboratory by Didier Cassereau. This software calculates the acoustic field produced by large arrays of transducers in complex media.

A. Imaging with the time reversal process

The time reversal process is exploited in order to produce a synthetic image of the sample, at the depth of the three flaws. The B-Scans measured along the y axis after two iterations (Fig. 9) are numerically backpropagated with the PASS code for the 50 positions of the array. Then, the 50 fields calculated along the x and y axis, are incoherently summed, taking into account the 1 mm array pitch between two consecutive measurements (Fig. 19). The image presents three maxima related to the reflectivity of each defect. Note that the 0.4 mm defect is detected with a 7.5 dB signal-to-noise ratio.

B. Imaging with the DORT method

The first "temporal eigenvector" obtained with DORT can be exploited as a B-Scan and thus numerically backpropagated. The first "temporal eigenvector" is backpropagated for the 50 positions of the array along the y axis, at a depth of 140 mm. The incoherent combination of the indi-

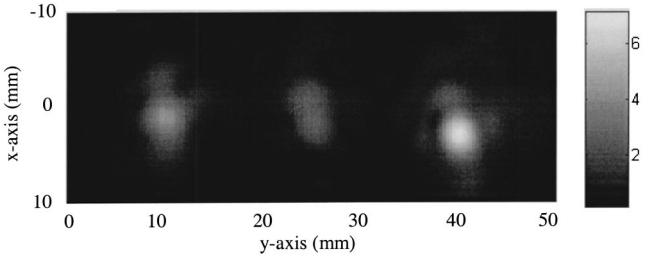

FIG. 20. Synthetic image of the sample at 140 mm depth obtained with the DORT method.

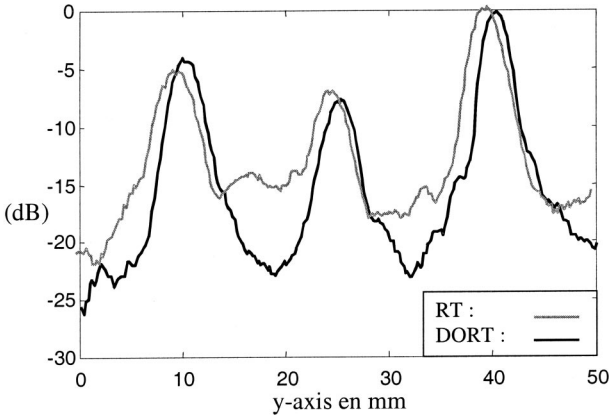

FIG. 21. Maximum of the projection of the two images along the y axis (dB).

vidual images calculated for each position of the array provides a complete image of the sample. Figure 20 is the synthetic image of the sample at the depth of the flaws. The three defects are detected with a good signal-to-noise ratio.

As shown in Fig. 21, the smallest flaw is detected 15 dB above the noise. The numerical backpropagation of the experimental data shows the efficiency of the DORT method in nondestructive testing to detect and locate a 0.4 mm diameter FBH in a noisy structure. This technique provides a synthetic image of the sample at a depth of 140 mm where the defects (including the 0.4 mm one) are well detected.

This study confirms the ability of the DORT method and of the time reversal mirror to detect small defects in a complex medium with a satisfactory signal-to-noise ratio.

VI. THE DORT METHOD IN A NOISE AREA

In Sec. IV C, we have applied the DORT method on 800 ns temporal window corresponding to the depth of the three defects. This detection technique is also applied to a defect free zone. The interelement impulse responses are acquired on a 4.2 μs temporal window, for 50 array positions ranging from 1 to 50 mm. For each position of the array, the transfer matrix is calculated on 18 temporal windows of 800 ns duration at 200 ns steps. This corresponds to depth ranging from 132 to 144 mm. After decomposition of the 50 times 18 matrices, the behavior of the singular values is analyzed.

The first singular value is represented at 5 MHz along the z and y axis, forming an image of the medium (Fig. 22). Three maxima associated with the defects of 0.8, 0.4, and 0.5 mm diameter appear around the depth $z=140$ mm for the positions $6\text{ mm}\leqslant y\leqslant 26\text{ mm}$, $28\text{ mm}\leqslant y\leqslant 33\text{ mm}$, and $41\text{ mm}\leqslant y\leqslant 49\text{ mm}$, respectively. Note that each flaw is detected for several temporal windows (5 for the 0.8 mm defect). This image also shows that a peak appears for several noise areas. In order to show the robustness of the DORT method, we now show that the peaks observed in noise areas cannot effectively correspond to any defect.

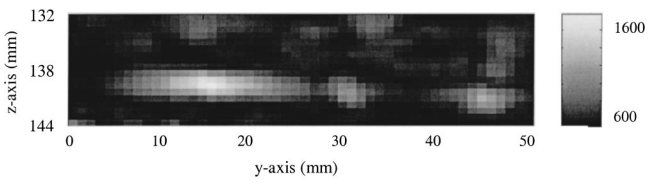

FIG. 22. Image of the medium with the first singular value calculated versus z and y axis.

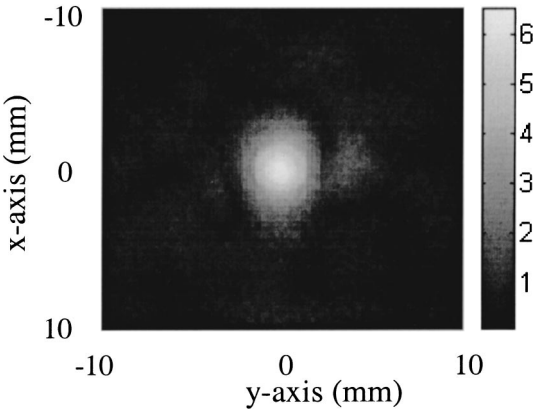

FIG. 23. Acoustic field versus x and y axis, obtained by backpropagation of the first "temporal eigenvector" at the depth of $z=132$ mm for the array position $y=33$ mm.

We numerically backpropagate the first eigenvector $v_1(t)$ corresponding to a noise area for several positions of the array. For instance, we choose to backpropagate $v_1(t)$ calculated for four array positions along the y axis ($y=32$, 33, 34, and 35 mm) and at the depth of $z=132$ mm (e.g., corresponding to the first temporal window). The acoustic field obtained by backpropagation of $v_1(t)$ for $y=33$ and 34 mm is represented along the x and y axis (Figs. 23 and 24). Note that the geometrical focal point is at the center of the image (e.g., for $x=y=0$ mm) for each backpropagation. For each array position ($32\text{ mm}\leqslant y\leqslant 35\text{ mm}$), the field calculated along $x=0$ axis presents a maximum at the focal point (Fig. 25).

Thus, the behavior of the DORT method is completely different in a high speckle zone than the zone around a defect. For the last case, the field is focused on the defect position. Consequently, when the array is translated for a 1 mm distance along the y axis, the distance between the two consecutive peaks is also equal to 1 mm. Moreover, the maximum associated with a defect coincides with the focal

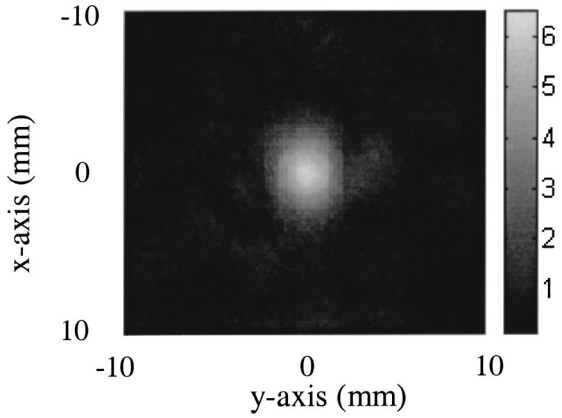

FIG. 24. Acoustic field versus x and y axis, obtained by backpropagation of the first "temporal eigenvector" at the depth of $z=132$ mm for the array position $y=34$ mm.

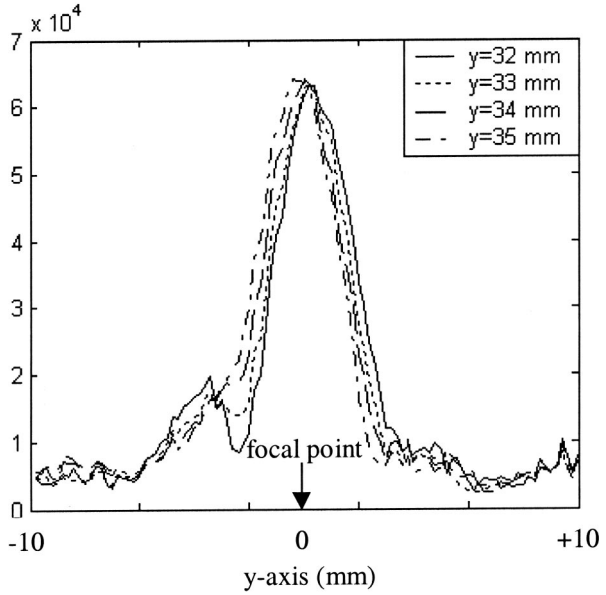

FIG. 25. Acoustic field along $x=0$ axis, obtained by backpropagation of the first ''temporal eigenvector'' at the depth of $z=132$ mm and for the array positions $y=31$, 32, 33, 34, 35 mm.

point only when the defect is at this point. Concerning the noise area, we have shown that the first eigenvector always focuses at the array focal point, because the array used for these experiments is prefocussed. This analysis allows us to discriminate the contribution of a defect from the speckle caused by the microstructure.

VII. CONCLUSION

Three techniques have been applied to the detection of FBH in a titanium billet, the standard transmit/receive focusing, the time reversal mirror and the DORT method. The DORT technique provides a real improvement in detection of deep weak defects in a noisy structure. On the synthetic images obtained by numerical backpropagation of the data with PASS, a 0.4 mm large and 140 mm deep defect was detected with a 15 dB signal-to-noise ratio using the DORT method whereas it was 7.5 dB for the time reversal process.

The sensitivity of each detection technique to a misalignment of the array relative to the liquid–solid interface has also been studied. The standard focusing technique does not allow a correct detection of the 0.8 mm flaw when the array is no longer adapted to the interface geometry. The sensitivity of the time reversal mirror is better than the standard focusing technique but worse than the DORT method. Thus, the DORT technique promises to be useful to detect flaws located in samples with complex geometry and using arrays which are not necessarily matched to this geometry.

We have also shown that the numerical backpropagation of the first eigenvector is a good test to get rid of false alarms. In a noise area presenting a peak on the first singular value, it appears that the backpropagation of the corresponding ''noise eigenvectors'' produces a peak which remains at the array focus while moving the array.

These detection techniques present several advantages and disadvantages. The DORT method and the standard transmit/receive focusing technique do not require programmable generators which are necessary for the time reversal process. The measurement of the interelement impulse responses for the DORT method provides information on the whole depth of the sample, whereas the iterative TR process requires an iteration for each short time windows. On the other hand, the DORT method requires N transmissions for N transducers, while the time reversal process only requires three transmissions. Therefore, further studies should focus on minimizing the data volume, measurements and calculations times.

This work does not answer the difficult question ''to what degree of inhomogeneities will the method remain efficient?'' Although some answer was given by Borcea *et al.*[19] in a theoretical and numerical analysis of a 2D fluid media, we believe that an answer to this question in the context of NDE should be the topic of further studies.

[1] A. Li, R. Roberts, F. J. Margetan, and R. B. Thompson, ''Study of the effect of microstructure on ultrasonic signal attenuation,'' in *Reviews of Progress in QNDE*, Vol. 20, edited by D. O. Thompson and D. E. Chimenti (Melville, New York, 2001), pp. 1322–1329.

[2] S. Chatillon, G. Cattiaux, M. Serre, and O. Roy, ''An ultrasonic system for the inspection of components with irregular geometry using a flexible phased array contact transducer and related processing algorithms,'' in *Reviews of Progress in QNDE*, Vol. 19, edited by D. O. Thompson and D. E. Chimenti (Melville, New York, 2000), pp. 1095–1102.

[3] P. J. Howard, D. C. Copley, J. D. Young, E. J. Nieters, and R. S. Gilmore, ''An improved methodology for the inspection of titanium alloys,'' IEEE Ultrason. Symp. Proc. **1**, 727–730 (1996).

[4] V. Lupien and F. Cancre, ''Ultrasonic phased array inspection of titanium billets,'' in *Reviews of Progress in QNDE*, Vol. 20, edited by D. O. Thompson and D. E. Chimenti (Melville, New York, 2001), pp. 919–926.

[5] C. W. Sherwin, J. P. Ruina, and R. D. Rawcliffe, ''Some early developments in synthetic aperture radar systems,'' IEEE Trans. Mil. Electron. **6**, 111–115 (1962).

[6] M. Karaman, P.-C. Li, and M. O'Donnell, ''Synthetic aperture imaging for small scale systems,'' IEEE Trans. Ultrason. Ferroelectr. Freq. Control **42**, 429–442 (1995).

[7] F. J. Margetan, H. Wasan, and R. B. Thompson, ''An experimental study of microstructure-induced ultrasonic signal fluctuations in jet-engine titanium alloys,'' in *Reviews of Progress in QNDE*, Vol. 19, edited by D. O. Thompson and D. E. Chimenti (Melville, New York, 2000), pp. 1433–1439.

[8] M. Fink, ''Time reversal of ultrasonic fields—Part I: Basic principles,'' IEEE Trans. Ultrason. Ferroelectr. Freq. Control, **39**, 555–566 (1992).

[9] F. Wu, J. L. Thomas, and M. Fink, ''Time reversal of ultrasonic fields-Part II: Experimental results,'' IEEE Trans. Ultrason. Ferroelectr. Freq. Control **39**, 567–578 (1992).

[10] M. Fink, C. Prada, and F. Wu, ''Self focusing in inhomogeneous media with time reversal acoustic mirrors,'' in *Proceedings of the IEEE Ultrasonic Symposium, 1989*, edited by B. R. McAvoy, 1989, Vol. 2, pp. 681–686.

[11] N. Chakroun, M. Fink, and F. Wu, ''Time reversal processing in ultrasonic nondestructive testing,'' IEEE Trans. Ultrason. Ferroelectr. Freq. Control **42**, 1087–1098 (1995).

[12] V. Miette, L. Sandrin, F. Wu, and M. Fink, ''Optimisation of time reversal processing in titanium inspections,'' IEEE Ultrason. Symp. Proc. **1996**, 643–647 (1996).

[13] C. Prada, J.-L. Thomas, and M. Fink, ''The iterative time reversal process: Analysis of the convergence,'' J. Acoust. Soc. Am. **97**, 62–71 (1995).

[14] N. Mordant, C. Prada, and M. Fink, ''Highly resolved detection and selective focusing in a waveguide using the D.O.R.T. method,'' J. Acoust. Soc. Am. **105**, 2634–2642 (1999).

[15] C. Prada, S. Manneville, D. Spoliansky, and M. Fink, ''Decomposition of the time reversal operator: Detection and selective focusing on two scatterers,'' J. Acoust. Soc. Am. **99**, 2067–2076 (1996).

[16] E. Kerbrat, R. K. Ing, C. Prada, D. Cassereau, and M. Fink, ''The D.O.R.T method applied to detection and imaging in plates using Lamb waves,'' in

Review of Progress in QNDE, edited by D. O. Thompson and D. E. Chimenti (Melville, New York, 2000), pp. 934–940.
[17] C. Prada and M. Fink, ''Separation of interfering acoustic scattered signals using the invariant of the time-reversal operator. Application to Lamb waves characterization,'' J. Acoust. Soc. Am. **104**, 801–807 (1998).
[18] D. Cassereau, ''Le retournement temporel en acoustique—Théorie et modélisation,'' thèse d'habilitation, Paris 7, 1997; see also http://www.loa.espci.fr/pass
[19] L. Borcea, G. Papanicolaou, C. Tsogka, and J. Berryman, ''Imaging and time reversal in random media,'' Inverse Probl. **18**, 1247–1279 (2002).